Key Points:
- Metrics are defined for ash hazards to aviation
- Methodology uses inverse modeling and satellite data
- Ash dosage is suggested as a useful parameter for aviation

Correspondence to:
A. J. Prata,
fred_prata@hotmail.com

Ash Metrics for European and Trans-Atlantic Air Routes During the Eyjafjallajökull Eruption 14 April to 23 May 2010

A. J. Prata[1] [ID], **N. Kristiansen[2,3]**, **H. E. Thomas[4]** [ID], **and A. Stohl[2]** [ID]

[1] AIRES Pty. Ltd, Mount Eliza, Victoria, Australia, [2] NILU, Kjeller, Norway, [3] The Met Office, Exeter, UK, [4] School of Earth Sciences, University of Bristol, Bristol, UK

Abstract Metrics for the risk associated with the threat that airborne volcanic ash particles pose to commercial jet aircraft are presented using simulations based on a Lagrangian particle transport and dispersion model driven by satellite measurements for the Eyjafjallajökull volcanic eruption, Iceland, for the period 14 April to 23 May 2010. The study utilizes a four-dimensional data set of simulated ash concentrations together with European and trans-Atlantic air routes to determine metrics corresponding to the total mass intercepted (defined as the dose), the mass interception rate (the dose rate), and the concentration (the exposure) over time (the dosage) that a jet aircraft encounters along the air route. The methodology can be used as a logistical and flight planning tool in a forecast mode and also in hindcast mode to assess the extent of airline fleet exposure to ash following an eruption, thereby providing operators with information useful for flight safety.

Plain Language Summary Volcanic ash that is dispersing in the atmosphere is a hazard to jet aircraft. We suggest new metrics for quantifying volcanic ash as a hazard to aviation by using a three-dimensional model/satellite data set derived for the 14 April to 23 May 2010 eruption of Eyjafjallajokull, Iceland. The metrics include dose rate, dose, dosage, and exposure. These are calculated for fictitious flight routes across Europe and for some trans-Atlantic routes. The methodology is globally applicable and may be of use to airlines, regulators, and other aviation stakeholders.

1. Introduction

When volcanoes erupt, they send particles and gases into the atmosphere. If the eruption is powerful enough, these materials can and do intersect air routes. A moderate-sized eruption can send several gigatons (Gt) of small particles (diameter < 6 μm) into the troposphere that can reach the tropopause. The particles, once embedded in the troposphere, are transported by the winds and can spread thousands of kilometers from the source. Dry and wet deposition and aggregation remove most of the large particles leaving behind a small but significant fraction of ash that once detached from the volcano can resemble meteorological clouds that are tracked using specialized satellite-based algorithms for many hours to days depending on the original amount of ash emitted and the four-dimensional (4-D) wind (Thomas & Watson, 2010). The portion of the size distribution remaining in the atmosphere is described well by a Gumbel distribution with a typical mean size of around 1–6 μm radius (Prata & Prata, 2012). It is well known that these particles can enter the hot parts of commercial jet engines and cause them to flame out and stall (Prata & Rose, 2015). The precise mechanisms by which engine damage is caused by ash particles are not entirely well understood, but the silicate (Si) composition of the ash and transition through a critical temperature that transforms the glassy part of the ash from solid to liquid is believed to be of primary importance (Song et al., 2016).

Commercial jet aircraft do not currently have any onboard instrumental means to detect airborne ash, and aircraft operators generally rely on satellite detection in near real time, most often by infrared sensors, and information from atmospheric dispersion models to predict the movement of the ash cloud. Improvements in the forecasting of the movement of ash in the atmosphere can be made using data assimilation (Fu et al., 2017), data insertion (Wilkins et al., 2016), and by inverse modeling (Stohl et al., 2011), which better characterizes the eruption source and thereby provides a better forecast. Satellite data are ideally suited for use in data assimilation and inverse modeling because of their global reach, timeliness, and recent improvements

of satellite retrievals of volcanic ash (Francis et al., 2012; Millington et al., 2012; Pavolonis, 2010). Ancillary data, for example, from ground-based lidar are also useful, when available, but unfortunately, over vast tracts of the Earth and especially the oceans such ground-based measurements are absent. Data from other aircraft and from *in situ* instruments are also valuable but in general not available. The shortcoming of the ability to accurately measure and forecast ash concentrations in volcanic clouds that intersect air routes has led to a very conservative approach to aviation safety, and this has an economic impact. Efforts to improve both measurements and modeling are ongoing, and there already exists a valuable data set developed during the April–May 2010 Eyjafjallajökull eruptions based on state-of-the science satellite-based ash retrievals and dispersion modeling (Stohl et al., 2011). Peterson and Dean (2008) first suggested using models to determine the relative exposure of aircraft to volcanic ash, and Kristiansen et al. (2015) performed a virtual fly-through for the single ash encounter flight during the Kelut eruption. They reported an estimated dosage of 1.2 g m^{-3} s. The purpose of our study is to use the results of the inverse modeling to determine how aviation may have been (or was) affected during the Eyjafjallajökull eruption by performing "virtual" flights through the 3-D data set. The paper is organized as follows: a brief description of the characteristics of the Eyjafjallajökull eruption, with respect to ash emissions to the atmosphere, is provided, followed by a description of the model/satellite data set. We refer to our simulation as a model/satellite data set because the full 3-D data set was generated by performing inversions based on actual satellite-based retrievals. The methodology used is described next, and we introduce the idea of the ash metrics: exposure, dosage, dose, and dose rate, providing their formal definitions. Results are presented by utilizing a database of air routes available publicly for popular European airlines during the period 14 April to 23 May 2010. We also consider some trans-Atlantic routes and assess their vulnerability during the Eyjafjallajökull ash crisis. Our discussion considers the advantages and disadvantages of our approach, and we suggest how the approach may be used in the future to assist in air route planning for the next eruption that affects European flights. While we have concentrated on European and trans-Atlantic air routes, our methods are quite general and may be applied to any other part of the world.

A small set of conclusions is presented, with some suggestions on how to improve the methodology and what further work is needed in order to make the tools operational.

2. The Eyjafjallajökull Eruption

Eyjafjallajökull (19°36′48″W, 60°37′12″N, 1,651 m above sea level) is an ice-covered stratovolcano situated in southern Iceland. During March 2010 the volcano became restless with a series of small fire-fountaining and lava-producing events. On 14 April 2010 the volcano erupted sending ash particles and SO$_2$ gas into a strong westerly wind that brought an ash and gas plume to the northern parts of western Europe by 15 April and in the next few days a weaker cloud to southern and eastern Europe, followed by a second emission in May (Gudmundsson et al., 2012; Stohl et al., 2011). European aviation was brought to a standstill for a period of 5 days in April, and further shutdowns of airspace occurred in May. Trans-Atlantic flights were also affected because of airspace closures in Europe. There are no validated reports of actual engine or airframe damage, but several airlines reported ash deposits in engine parts and airframes and the likelihood of ash/aviation encounters would (presumably) have been high if aircraft had not been grounded. Various estimates of the amount and spread of the volcanic ash are available. Gudmundsson et al. (2012) estimated a total release of ~70 Tg of very fine ash (radius < 28 μm), while Stohl et al. (2011) estimated ~11 Tg. The large discrepancy between the two estimates has not been resolved and illustrates the high degree of uncertainty associated with measurements and modeling of dispersing very fine ash. Figure 1 shows a set of Spin Enhanced Visible and InfraRed instrument (SEVIRI)-based ash retrievals for six different dates giving an indication of the intermittent coverage and spatial extent of the ash clouds over Europe, the North Sea, and the North Atlantic. These passive infrared retrievals are available at 15-min intervals continuously over the European region and have been used extensively to study this eruption and others. The retrieval methodology and further examples from SEVIRI and other infrared satellite instruments can be found in various studies (Francis et al., 2012; Pavolonis, 2010; Prata & Grant, 2001; Prata & Prata, 2012). Note that these data only show the horizontal spread of the ash: no vertical information is available in these passive infrared-based satellite retrievals. Since satellite data can only ever provide a picture of the ash at the time the measurements are made, it is necessary to use a forecast model for planning purposes and risk assessment (Dacre et al., 2011). Ash transport and dispersion models rely on the characteristics of the source (e.g., source strength, vertical and temporal structures,
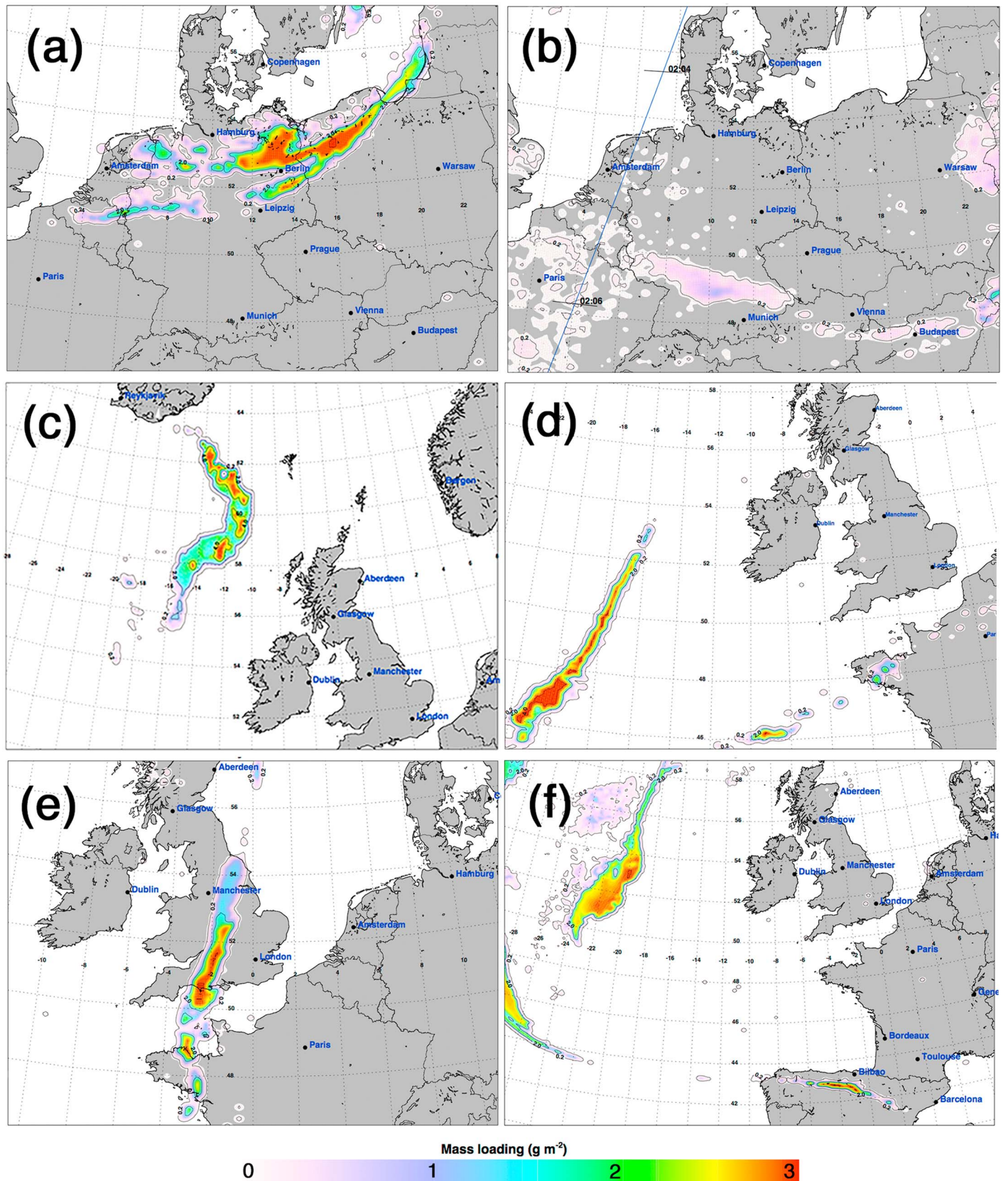
Figure 1. Satellite retrievals of ash mass loadings on various days and times during the Eyjafjallaökull eruption. (a) 16 April 09:00 UT. (b) 17 April 02:30 UT. (c) 6 May 17:00 UT. (d) 8 May 07:00 UT. (e) 12 May 06:30 UT. (f) 15 May 06:00 UT.

Table 1
Particle Size Fractions and Corresponding Settling Velocities Used in the FLEXPART Model

Diameter (μm)	Fraction	Average settling velocity (ms^{-1} × 10^{-3})
4.0	0.23	1.652
6.0	0.25	3.672
8.0	0.17	6.487
10.0	0.12	10.098
12.0	0.09	14.504
14.0	0.06	19.706
16.0	0.04	25.704
18.0	0.03	32.498
25.0	0.01	62.542

Note. Settling velocities in FLEXPART are calculated online and depend on air density and the temperature-dependent dynamic viscosity of the air (Naeslund & Thaning, 1991). The values in Table 1 are default values for standard atmospheric conditions.

and particle size distribution) which are generally poorly constrained so an inversion scheme was developed by Eckhardt et al. (2008), Kristiansen et al. (2012), and Stohl et al. (2011) to utilize the satellite measurements to estimate the source parameters. The resulting model data sets are described next.

3. Data Sets

3.1. Model

These data include dispersion model output for the Eyjafjallajökull eruption in 2010, from 14 April to 23 May at hourly intervals. The model used is the Lagrangian Particle Dispersion Model FLEXPART version 9.0 (https://www.flexpart.eu/). The satellite/model simulation uses the *a posteriori* ash source term determined from inverse modeling (see Kristiansen et al., 2012 and Stohl et al., 2011). The ash particle size distribution used in the simulation includes nine size bins described in Table 1.

3.2. Meteorological Data

The model uses Integrated Forecasting System meteorological forecast data from the European Centre for Medium-Range Weather Forecasting, with 3-hourly time resolution, 1.0 × 1.0° horizontal resolution, and 92 vertical levels from the surface to the stratosphere and a nested higher resolution (0.18 × 0.18°) over Europe (−36° to 36° longitude, 36° to 72° latitude).

3.3. Air Routes Data

The source of air route information is a free resource available from https://flightplandatabase.com/planner. The data resource allows us to investigate both European and trans-Atlantic routes and gives a much broader selection of flight paths than using, for example, air routes based on data from a single airline. From these routes we can calculate exposures, dosages, dose rates, and doses (see section 4) that were encountered during the eruption crisis. An example of an air route taken from the resource for a flight across the North Sea from Keflavik airport, Iceland, to Stockholm, Sweden, is shown in Figure 2. Generally, the number of data points (waypoints) on the air route is small and it is useful to interpolate the data on great circles to a more dense data set that is consistent with the model/satellite data set.

4. Definitions

Within the scientific literature and also in common use, the terms *dose*, *dosage*, *exposure*, and related or derivative terminologies do not have a uniformly accepted definition. This particularly applies to dose and dosage where the terms are often used interchangeably or to mean the same thing. In air pollution studies, medical research and radioactive radiation studies the terms that are inconsistently defined. For the purpose of this work we make the following definitions, specifically related to volcanic ash intercepted by an aircraft:

1. Dose rate, $\mathbf{D}_t$. The amount (mass) of pollutant ingested per unit time. The units are mass per unit time (kg s^{-3}).
2. Dose, $\mathbf{D}$. The dose rate integrated over a time interval. The units are mass (kilogram).
3. Exposure, $\mathbf{E}$. Equal to the mass concentration of pollutant (here we refer specifically to volcanic ash). The units are mass per unit volume (kg m^{-3}).
4. Dosage, $\mathbf{D}_o$. The concentration of pollutant exposure accumulated over a period of time. The units are mass per volume integrated over time (kg m^{-3} s).

These definitions make no assumptions about the processes affecting the ash once it has entered the engine.

5. Methodology

Prata and Prata (2012) suggested that ash concentrations as determined by models and ash mass loadings, as determined by satellites, do not provide sufficient information on which to base an estimate of the potential risk to an aircraft encountering an ash cloud (or plume). A meaningful measure of the hazard is a dosage, $\mathbf{D_o}(\delta t)$. Figure 3 shows an aircraft in 3-D space with position represented by Cartesian coordinates x, y, and z at time t, and c is the concentration of volcanic ash. δt is the time the aircraft spends in the ash cloud
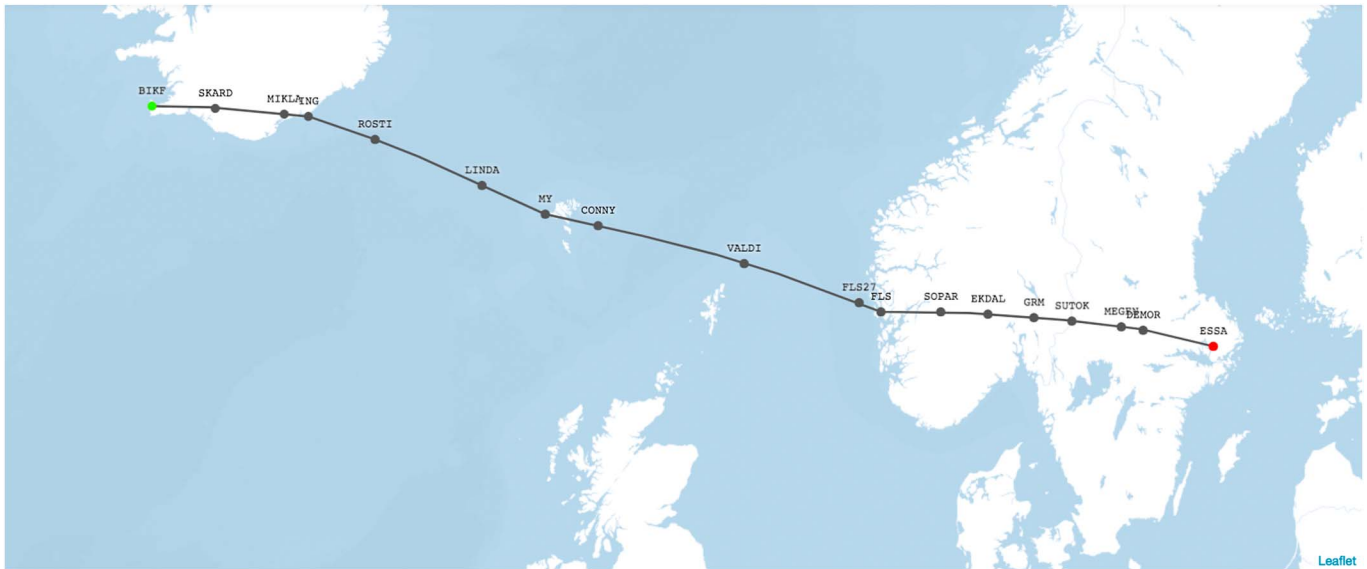
| ID	Type	Via	Altitude	Latitude	Longitude	Leg Dist	Tot Dist	Heading (true)	Name
O BIKF	APT	–	0 ft / 0 m	63.98161°	−22.61456°	–	0 nm	–	Keflavik
• SKARD	FIX	–	22,700 ft / 6,919 m	63.94278°	−20.20500°	63 nm	63 nm	91° / 93°	–
• MIKLA	FIX	G3 (AWY-LO)	35,000 ft / 10,668 m	63.84833°	−17.57417°	69 nm	133 nm	93° / 96°	–
• ING	VOR	G3 (AWY-LO)	35,000 ft / 10,668 m	63.80306°	−16.63806°	24 nm	158 nm	96° / 97°	INGO VOR-DME
• ROSTI	FIX	G3 (AWY-LO)	35,000 ft / 10,668 m	63.40639°	−14.11222°	71 nm	229 nm	108° / 111°	–
• LINDA	FIX	G3 (AWY-LO)	35,000 ft / 10,668 m	62.62167°	−10.00000°	121 nm	351 nm	111° / 115°	–
• MY	NDB	G3 (AWY-LO)	35,000 ft / 10,668 m	62.10694°	−7.58778°	73 nm	425 nm	114° / 116°	MYGGENES NDB
• CONNY	FIX	G3 (AWY-LO)	35,000 ft / 10,668 m	61.90000°	−5.58333°	57 nm	483 nm	102° / 103°	–
• VALDI	FIX	G3 (AWY-LO)	35,000 ft / 10,668 m	61.21417°	0.00000°	164 nm	648 nm	102° / 107°	–
• FLS27	FIX	G3 (AWY-LO)	35,000 ft / 10,668 m	60.47194°	4.38361°	135 nm	783 nm	107° / 111°	–
• FLS	VOR	–	35,000 ft / 10,668 m	60.31126°	5.21219°	26 nm	810 nm	111° / 112°	FLESLAND VOR-DME
• SOPAR	FIX	N623 (AWY-LO)	35,000 ft / 10,668 m	60.29556°	7.50000°	68 nm	878 nm	90° / 92°	–
• EKDAL	FIX	N623 (AWY-LO)	35,000 ft / 10,668 m	60.25556°	9.32222°	54 nm	932 nm	92° / 93°	–
• GRM	VOR	N623 (AWY-LO)	35,000 ft / 10,668 m	60.19176°	11.07442°	52 nm	984 nm	93° / 95°	GARDERMOEN VOR-DME
• SUTOK	FIX	P607 (AWY-LO)	35,000 ft / 10,668 m	60.12750°	12.51278°	43 nm	1028 nm	95° / 96°	–
• MEGEN	FIX	P607 (AWY-LO)	23,300 ft / 7,102 m	60.01833°	14.40856°	57 nm	1085 nm	96° / 97°	–
• DEMOR	FIX	P607 (AWY-LO)	17,900 ft / 5,456 m	59.96125°	15.24542°	25 nm	1110 nm	97° / 98°	–
O ESSA	APT	–	0 ft / 0 m	59.65014°	17.94363°	83 nm	1194 nm	102° / 104°	Stockholm Arlanda

Altitude Profile
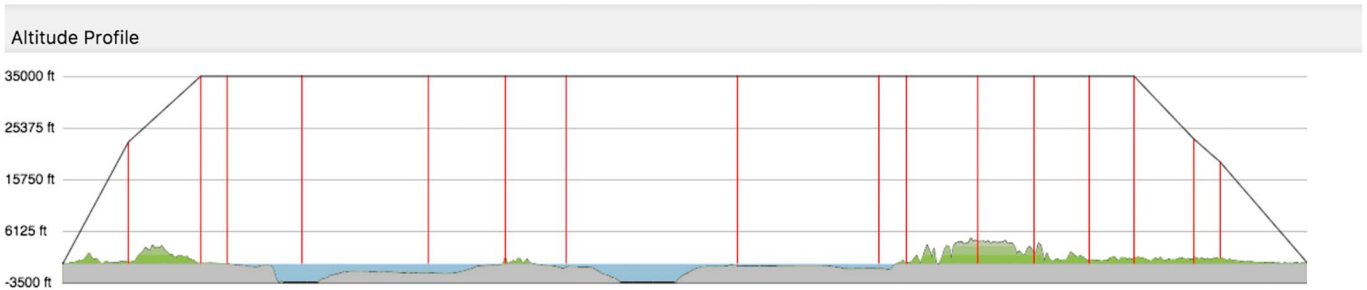
Figure 2. Flight route data for the air route from Keflavik, Iceland, to Stockholm, Sweden.

as it traverses the path from l_o at time t_o to l_1 at time t_1, the starting and ending points ($\delta l = |l_1 - l_o|$), respectively, along the air route. The dose rate $\mathbf{D}_t$ is

$$\mathbf{D}_t = \mathbf{E}Av(t), \tag{1}$$

where A is the cross-sectional area of the engine entrance, E is the exposure (or concentration of ash), and $v(t)$ is the airspeed at time t. In words, the dose rate is equivalent to the concentration (c) of ash integrated over the area of the engine inlet, multiplied by the airspeed of the aircraft at time t. The dose ($\mathbf{D}$) an engine experiences over a time interval δt follows by integrating the dose rate over time:

$$\mathbf{D}(t, t + \delta t) = \int_t^{t+\delta t} \mathbf{D}_t dt. \tag{2}$$
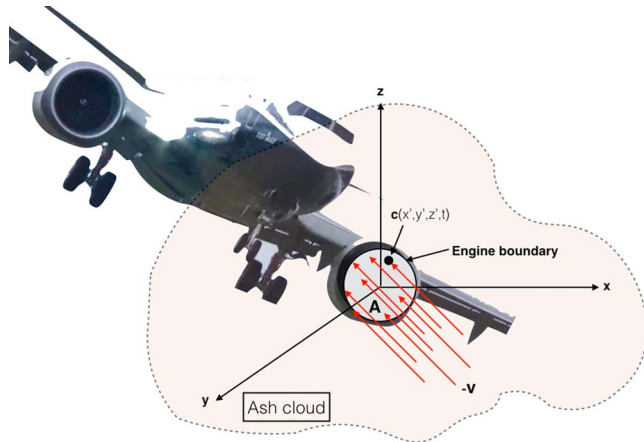
Figure 3. Schematic showing the intersection of a volcanic ash cloud with the engines of a commercial jet aircraft with ground speed v. The concentration at $c(x', y', z', t)$ at time t varies with position coordinates x', y', and z', and it is assumed that this is admitted at the boundary of the engine, simplified as a circular disc. The ash cloud's velocity vector is assumed negligible in comparison to the aircraft ground speed.

The dosage is the integration of the exposure over the time interval δt

$$\mathbf{D_o}(t, t + \delta t) = \int_t^{t+\delta t} \mathbf{E}(x, y, z, t)\mathrm{d}t \tag{3}$$

and is equivalent to the concentration of ash that the aircraft is exposed to. The exposure can also be defined as

$$\mathbf{E} = \frac{\partial \mathbf{D_o}}{\partial t}. \tag{4}$$

The units of $\mathbf{D_o}(t, t + \delta t)$ defined this way are kg m^{-3} s. These definitions have some intuitively sensible attributes. The dose corresponds to the mass of volcanic ash that can be intercepted at the boundary of the engine, while the dose rate measures how much of that mass is intercepted per unit time. Dose rate measures the *admission* of matter entering the engine at its boundary. As suggested before this metric is related to potential engine damage but not a direct measure of it because of internal engine processes that affect the ash as it transits through the engine. The dosage may be an important metric because it measures the exposure of the engine to the concentration field over a period of time. It is not known whether an engine fails because of an accumulation of a critical mass of ash or whether the rate of mass ingestion is critical. A simple illustration of the problem is provided in Figure 3 which shows an idealized cross section of the entrance boundary of an engine, represented by a disc, traveling at the aircraft velocity $-v$ within an ash cloud that has a much smaller (negligible) velocity (This simplification has no effect on the main results of the study as it is straightforward to use the resultant vector velocity, if all velocity vectors are known.) In the calculations that follow, the diameter of the engine is assumed to be 3.2 m and the cruising airspeed is assumed to be 950 km hr^{-1} ($\sim$250 m s^{-1}), and the airspeed on descent and climb is assumed to be 300 km hr^{-1} ($\sim$80 ms^{-1}). The disc intersects an area of the ash cloud A corresponding to the cross-sectional area of the engine entrance where the concentration is c and is assumed to vary everywhere within the cloud. Equations (1)–(3) can be used to estimate the ash metrics based on model simulations.

In the case when concentrations from modeling are not available, real-time measurements are needed. In situ measurements of ash concentration can also be used with the metrics given above. In that case (1)–(3) can also be used directly and the main source of error (apart from instrumental measurement uncertainty) lies with the assumption of uniformity at scales of meters (the scale of the engine boundary) compared to the instrument measurement scale which is likely to be different.

Measurements of the thickness of the ash cloud in the direction of travel are very difficult to make, but a measure of the mass loading (mass per unit area, $m_z(x, y)$) of the ash cloud may be known from a satellite measurement looking downward onto the ash cloud. If the ash cloud has a uniform concentration within the vertical column sampled by the satellite and the thickness of the ash cloud is known, the uniform concentration can be estimated. The vertical thickness can be estimated from a satellite (or coincident ground based) lidar measurement. If the mass loading in the flight direction (m_l) can be measured, then an alternate method to estimate the dose rate follows, since:

$$c(x, y, z) = m_l / \delta l,$$

where δ_l is the thickness in the line of sight. The dose rate can then be calculated immediately from

$$\frac{\mathrm{d}D}{\mathrm{d}t} = m_l A \frac{v}{\delta l}. \tag{5}$$

The terms on the right-hand side of (4) can be evaluated without knowing the concentration of the ash if a measurement of m_l is available (e.g., from an onboard remote sensing instrument). The total mass intercepted is simply $A \times m_l$, and the mass loading along the path $l(x, y, z)$ is

$$\overline{m}_l(t) = \int_{l_o}^{l_1} c(x, y, z, t)\mathrm{d}l;$$

Table 2
Origin, Destination, Distance, and Number of Waypoints for the Set of Air Routes Used in This Study

Origin	ICAO code	Destination	ICAO code	Distance (km)	No. of waypoints
Keflavik	BIKF	Stockholm	ESSA	2,147	16
Keflavik	BIKF	Madrid	LEMD	2,894	22
Keflavik	BIKF	Rome	LIRF	3,322	52
Keflavik	BIKF	Moscow	UUEE	3,322	27
Keflavik	BIRK	Copenhagen	EKCH	2,117	17
Keflavik	BIRK	Milan	LIMC	2,793	36
Brussels	EBBR	Copenhagen	EKCH	754	9
Berlin	EDDB	Keflavik	BIKF	2,434	19
Berlin	EDDB	Madrid	LEMD	1,854	36
Hamburg	EDDH	Berlin	EDDB	275	3
Hamburg	EDDH	Munich	EDDM	601	10
Luton	EGGW	Keflavik	BIRK	1,847	20
Luton	EGGW	Munich	EDDM	951	9
Luton	EGGW	Berlin	EDDT	933	14
Luton	EGGW	Manchester	EGCC	209	3
Luton	EGGW	Copenhagen	EKCH	950	10
Luton	EGGW	Oslo	ENGM	1,166	16
Luton	EGGW	New York	KJFK	5,538	23
Luton	EGGW	Barcelona	LEBL	1,192	18
Luton	EGGW	Milan	LIMC	962	14
Luton	EGGW	Prague	LKPR	1,042	20
Gatwick	EGKK	Boston	KBOS	5,275	22
Heathrow	EGLL	Berlin	EDDB	964	13
Heathrow	EGLL	Frankfurt	EDDF	653	10
Heathrow	EGLL	Hamburg	EDDH	746	8
Heathrow	EGLL	Munich	EDDM	943	8
Heathrow	EGLL	Manchester	EGCC	243	4
Heathrow	EGLL	Oslo	ENFB	1,164	17
Heathrow	EGLL	New York	KJFK	5,546	25
Oslo	ENGM	Munich	EDDM	1,319	25
Vilnius	EYVI	Heathrow	EGLL	1,748	23
Frankfurt	EDDF	Boston	KBOS	5,894	32
Frankfurt	EDDF	San Francisco	KSFO	9,158	41
Munich	EDDM	Rome	LIRF	729.3	13
Helsinki	EFHF	Los Angeles	KLAX	9,032	63
Helsinki	EFHF	Seattle	KSEA	7,690	49
Manchester	EGCC	Vancouver	CYVR	7,346	37
Luton	EGGW	Cairo	HECA	3,554	37
Luton	EGGW	Catania	LICC	2,008	39
Heathrow	EGLL	Montreal	CYUL	5,221	24
Heathrow	EGLL	Vancouver	CYVR	7,587	39
Heathrow	EGLL	Glasgow	EGPF	555	6
Heathrow	EGLL	Edinburgh	EGPH	534	6
Heathrow	EGLL	Dublin	EIDW	450	4
Heathrow	EGLL	Warsaw	EPWA	1,471	22
Heathrow	EGLL	Washington	KIAD	5,909	37
Heathrow	EGLL	Los Angeles	KLAX	8,770	52

Table 2 (continued)

Origin	ICAO code	Destination	ICAO code	Distance (km)	No. of waypoints
Heathrow	EGLL	Miami	KMIA	7,117	35
Heathrow	EGLL	Chicago	KORD	6,351	32
Heathrow	EGLL	Paris	LFPO	366	3
Dublin	EIDW	Copenhagen	EKCH	1,241	18
Dublin	EIDW	Boston	KBOS	4,809	14
Copenhagen	EKCH	Amsterdam	EHAM	633	7
Oslo	ENGM	Keflavik	BIKF	1,784	12
Oslo	ENGM	Tenerife	GCXO	4,088	43
Warsaw	EPWA	Amsterdam	EHAM	1,103	16
Stockholm	ESSA	Montreal	CYUL	5,877	31
Paris	LFPO	Berlin	EDDB	886	8
Paris	LFPO	Dublin	EIDW	798	19
Paris	LFPO	Boston	KBOS	5,540	20
Paris	LFPO	Seattle	KSEA	8,076	47
Paris	LFPO	Mexico	MMMX	9,208	62
Prague	LKPR	Amsterdam	EHAM	707	10
Guadeloupe	TFFR	Paris	LFPO	6,759	28

it follows that

$$\mathbf{D_o}(\delta l) = \frac{\overline{m_l}}{v}.$$

This shows that an onboard instrument capable of measuring the mass loading in the flight direction of the aircraft (i.e., viewing in the direction of the aircraft's velocity vector) would provide a direct estimate of the dosage encountered. Aircraft maneuvers and viewing constraints (e.g., viewing during ascent and descent or meteorological cloud between the aircraft and ash cloud) are important caveats, but in any case currently there are no onboard instruments capable of providing measurements of $\bar{m}_l(t)$ or $c(x, y, z, t)$.

5.1. Interpolations

There are two data sets required for the analysis: An air route consisting of waypoints that have been linearly interpolated at 0.25° longitude and latitude increments and the 4-D model/satellite data set that consists of concentrations at x, y, z in hourly increments. The process then involves flying the virtual aircraft along the air route through the 4-D model/satellite data field and calculating $\mathbf{D}_t$ and $\mathbf{E}$ as a function of position along the path. Since the aircraft is traveling at some (unknown) velocity an assumption must be made. For the air routes, the aircraft velocity is a free parameter and we are able to change this and study the effect of air speed on dosage along the air route. An efficient interpolation scheme was developed to include the effect of time of travel on the calculations for air routes that last longer than 1 hr, the basic time interval for our data.

The data set is readily amenable to calculations of $\mathbf{E}$, $\mathbf{D_o}$, $\mathbf{D}$, and $\mathbf{D}_t$ once the 3-D path of the aircraft (the air route) is known.

6. Results

Flight routes (see Table 2) were selected based on the satellite observations of the horizontal spread of ash from Eyjafjallajökull. Figure 4 shows the spatial pattern of the spread of ash using SEVIRI satellite observations (Prata & Prata, 2012) during the three major periods of eruptive activity: 14–17 April, 18 April to 4 May, and 5–18 May. SEVIRI ash retrievals were limited to a geographical region bounded by longitudes 30°W to 30°E and latitudes 30°N to 70°N. A set of 64 air routes were chosen so that they intersected the horizontal region of air space where ash was observed, but note that it is not possible from the observations to determine the vertical region. The number (64) and the air routes are of course arbitrary; we could equally have selected all the air routes operated by one airline or all the routes to and from Keflavik, for example. Any combination
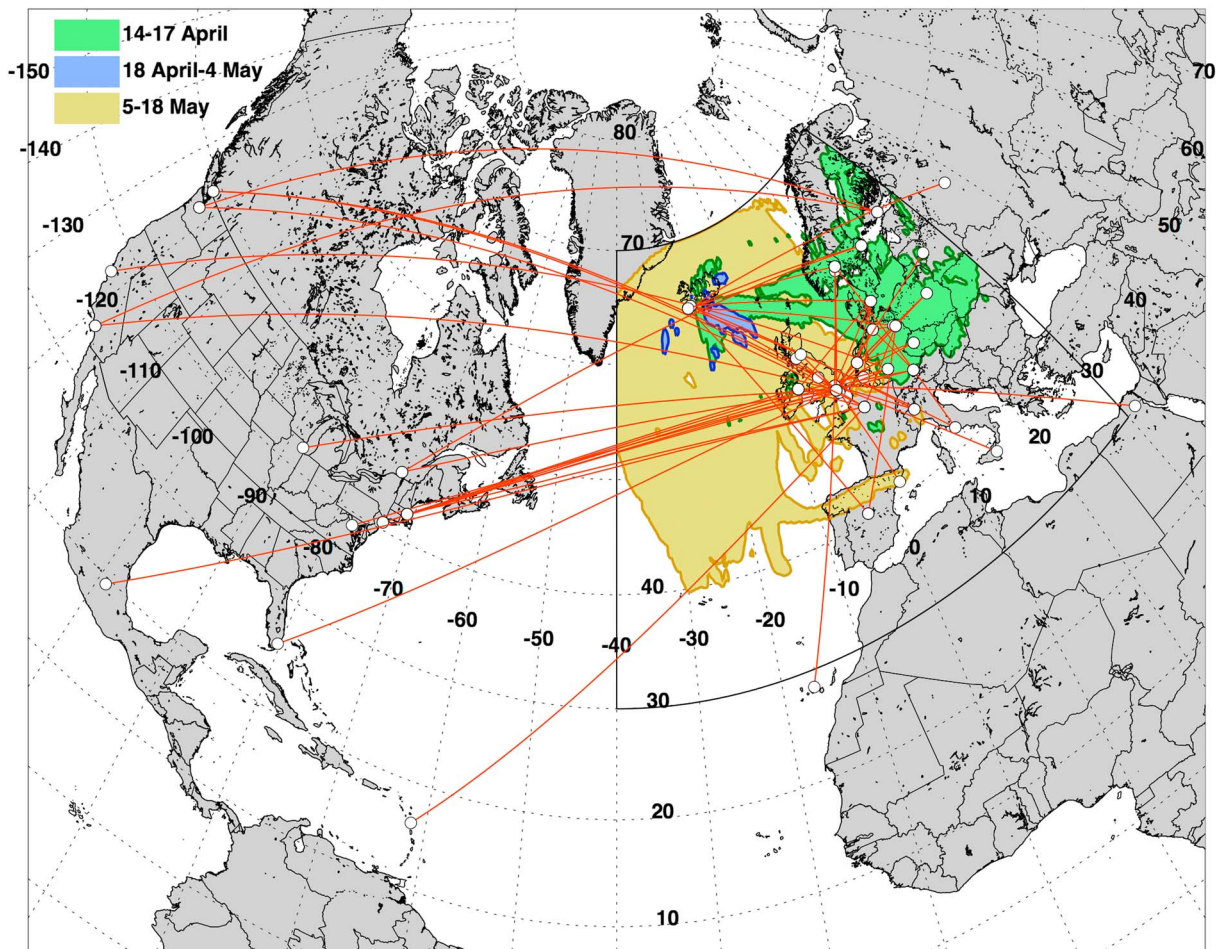
Figure 4. Horizontal spread of ash for the three main periods of eruptive activity during the Eyjafjallajökull eruption in April and May 2010. The great circle air routes (64) selected as "virtual fly-throughs" of the 4-D model/data set are indicated by the red lines. In the calculations, interpolated waypoints are used; great circle routes are shown for clarity.

of origin and destination air route is possible in the simulations. As we show in these results in fact different choices do not affect the main conclusion.

Analyses were made for each of the 64 flight routes flown on 15 April to 23 May assuming a departure on the hour, each hour throughout each day. The majority of flights did not occur in reality, but the temporal and spatial coverage of these virtual flights through the model data set are sufficient to capture any encounters, should they have occurred in reality. The flight route data contain the 3-D position of the aircraft at a typical temporal resolution of tens of minutes (the precise resolution depends on the flight duration). As the aircraft ascends and descends quite rapidly in comparison to time spent at cruise altitude, the takeoff and landing time periods are particularly sensitive to the location of the ash. Moreover, because in the case of Eyjafjallajökull the ash remained at relatively low altitudes, mostly below 25,000 ft, most encounters only happened during the takeoff and landing phases and were often rapid transits through the ash layers.

A typical calculation for the route shown in Figure 2 is provided in the panels of Figure 5. The flight is fictitious but follows an air route that is based on the flight planning information from the air routes database. For this calculation only one satellite/model simulation was used, representing the ash concentrations in the atmosphere for a 1 hr time interval centered at 17:00 UT on 15 April 2010. This was a time when ash was observed by satellite to be traveling eastward toward the northern parts of continental Europe. The left-hand panels show the flight with the planned cruise altitude of 35,000 ft. On this air route the aircraft experiences quite low ash concentrations as most of the ash is below the aircraft. Only when the aircraft begins to descend on its approach to Stockholm Arlanda airport does it encounter ash exposures >200 µg m^{-3},
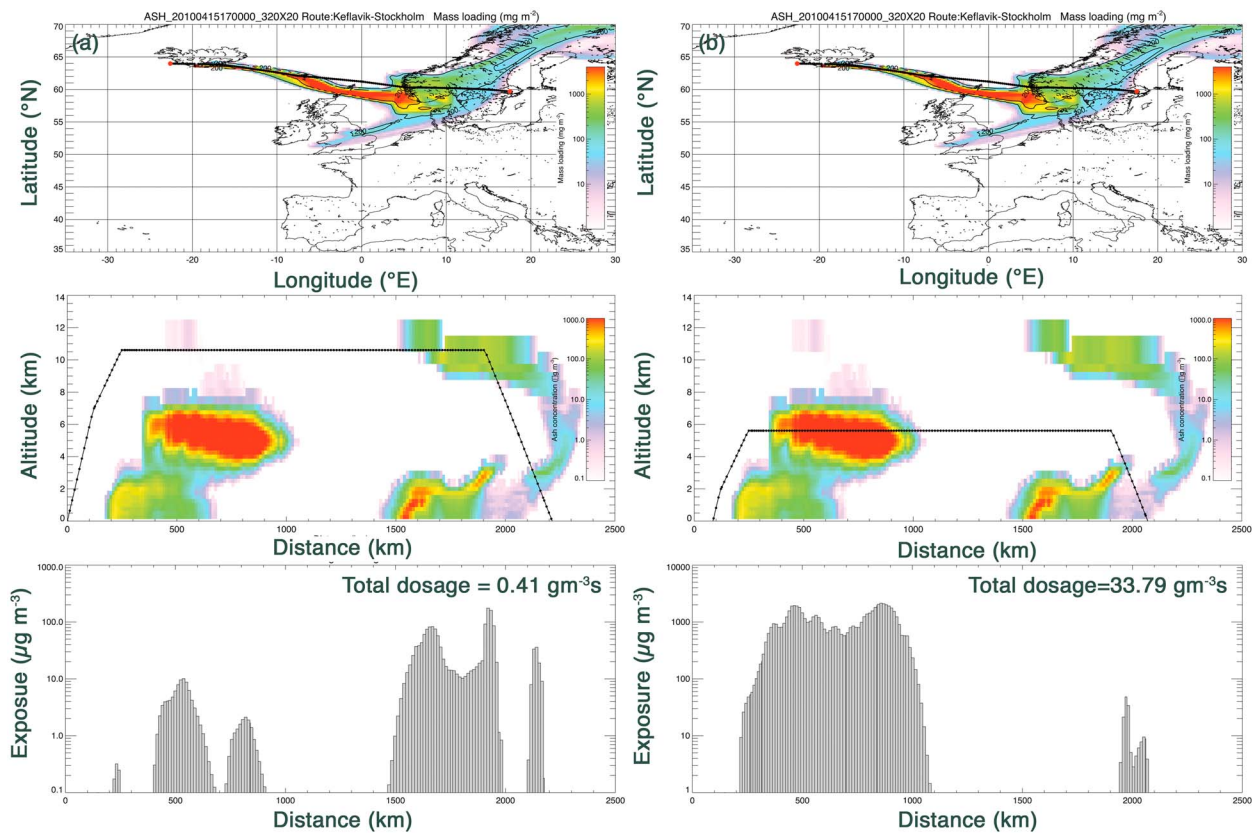
Figure 5. (a) From top to bottom: ash mass loadings, concentrations, and dosages for a flight from Keflavik to Stockholm on 15 April 2010. The total flight time is ~2 hrs 30 min covering a distance of ~2,100 km. (b) The same flight but with the cruise altitude artificially lowered from 35,000 to 18,500 ft. Notice the different scales used for the exposure in the two bottom panels.

corresponding to a dosage of 0.47 g m^{-3} s. The right-hand panels show the situation had the aircraft flown at a much lower cruise altitude of 18,500 ft. In this case the aircraft enters a highly concentrated part of the ash cloud and the dosage of ~33 g m^{-3} s, more than 50 times greater than when flying at 35,000 ft. Current Rolls-Royce advice (Rolls-Royce, 2016) is that a dosage of 14.4 g m^{-3} s may cause damage to engines. This value is calculated from an aircraft operating in an actual exposure of 2 mg m^{-3} ash concentration over a period of 120 min and does not consider processes occurring in the combustion chamber of the engine. This example highlights a potential risk for flights crossing the North Sea as the pilot must decide whether to proceed or return, as both options are equidistant. It also serves to show that if sufficiently robust information on the 3-D location (and movement) of the ash cloud is available to the pilot, then it is possible to avoid the ash cloud by altering only the flight altitude. This appears to be the option of lowest risk because ash clouds are known to form as thin vertical layers with thicknesses of a few 100 m to perhaps 3,000 m (Prata et al., 2015, 2017). Altering flights to higher/lower flight levels and/or also changing course in the crowded airways over Europe may not always be possible, but at least having such options available should reduce the risk of exposure to ash. The scenarios analyzed here assume a satellite/model concentration field that is representative of a 1 hr time interval. No attempt was made to dynamically adjust the ash concentrations with time to match the aircraft time, as the majority of flights are of short duration (<3 hr). Nevertheless, timing is important as the Eyjafjallajökull ash cloud of 15 April 2010 was traveling eastward at a mean velocity of ~50 km hr^{-1} so that an aircraft on descent may miss or pass through the ash cloud depending on the exact timing. This can be seen in Figure 6 where we have plotted the exposure for the Keflavik-Stockholm route at 16:00, 17:00, and 18:00 UT model times on 15 April 2010. This suggests that it may be possible to specify an "optimum time window," that is, a time period when the maximum number of flights could complete their route while remaining below the 14.4 g m^{-3} s dosage.
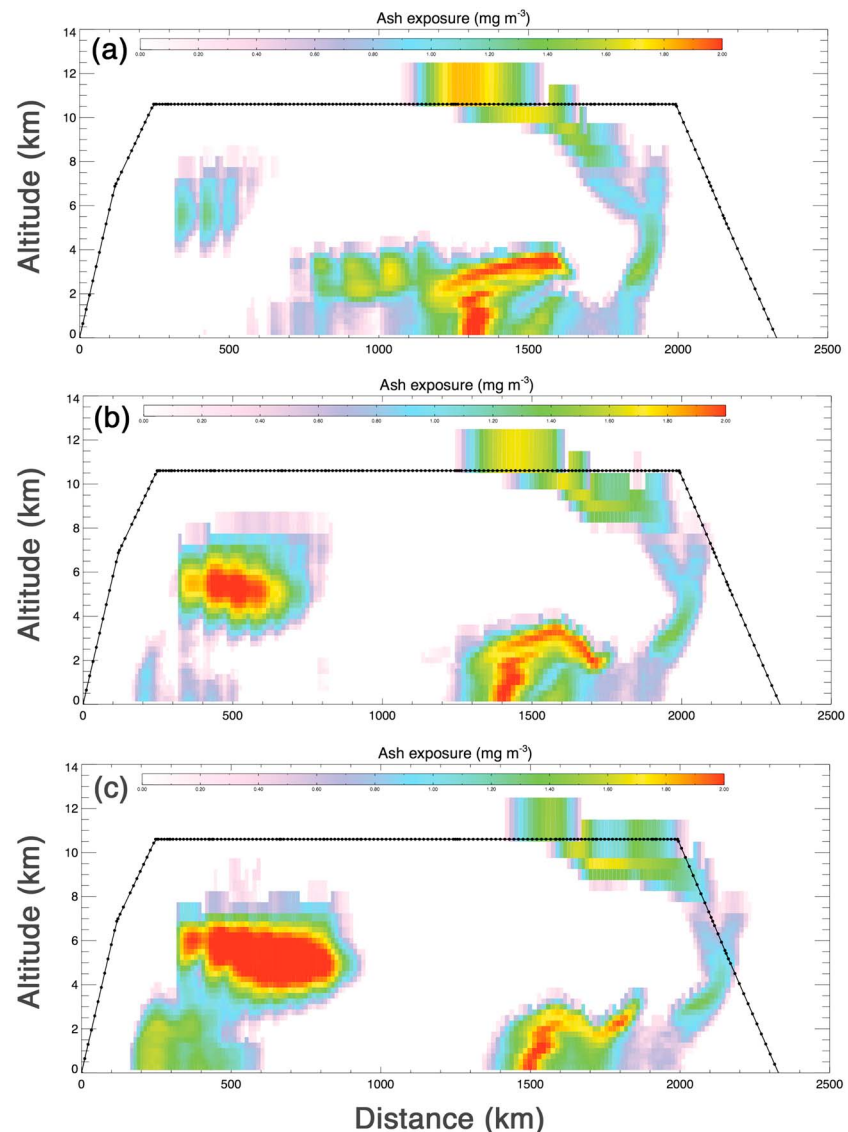
Figure 6. Exposures for three different model times: (a) 12:00, (b) 14:00, and (c) 16:00 UT on 15 April 2010. The dosages for these three times are 1.58, 0.97, and 0.51 g m^{-3} s, respectively.

6.1. Dosages and Doses

To get an overall picture of the ash hazard to aircraft over European and trans-Atlantic flight paths, the data for all 64 air routes have been analyzed by day and hour of day. Cumulative dosages and doses were calculated within each hourly interval and partitioned into European or trans-Atlantic routes. Constant cruise/descent/ascent speeds were assumed for all flights, and this leads to a linear correlation between the dosage and dose. In practice, aircraft may travel at different speeds on different flight routes and these may vary during the flight, especially during ascent and descent, takeoff and landing, or during holding situations. There were 21 trans-Atlantic air routes analyzed in total. The analysis shows which days and which hours within the days were more or less affected by the dispersion of the ash clouds. The results are shown in Figures 7 and 8 and shown in sequences of four consecutive days, with gray bars indicating the total for all routes and the blue bars for trans-Atlantic routes only. The first two sequences are for the period 15–22 April, during phase 1 of the eruption when the ash traveled rapidly eastward and then southward over continental Europe (see Figure 4). The main hazard (high dosages and doses) occurs during the early hours of 15 April, when high concentrations of ash were streaming eastward and mostly affecting air routes to and from Iceland. Some air routes using polar airways were also affected, as evidenced by the higher trans-Atlantic dosage shown in blue on the plots. By 16–18 April the cumulative amounts have decreased and also the hazard
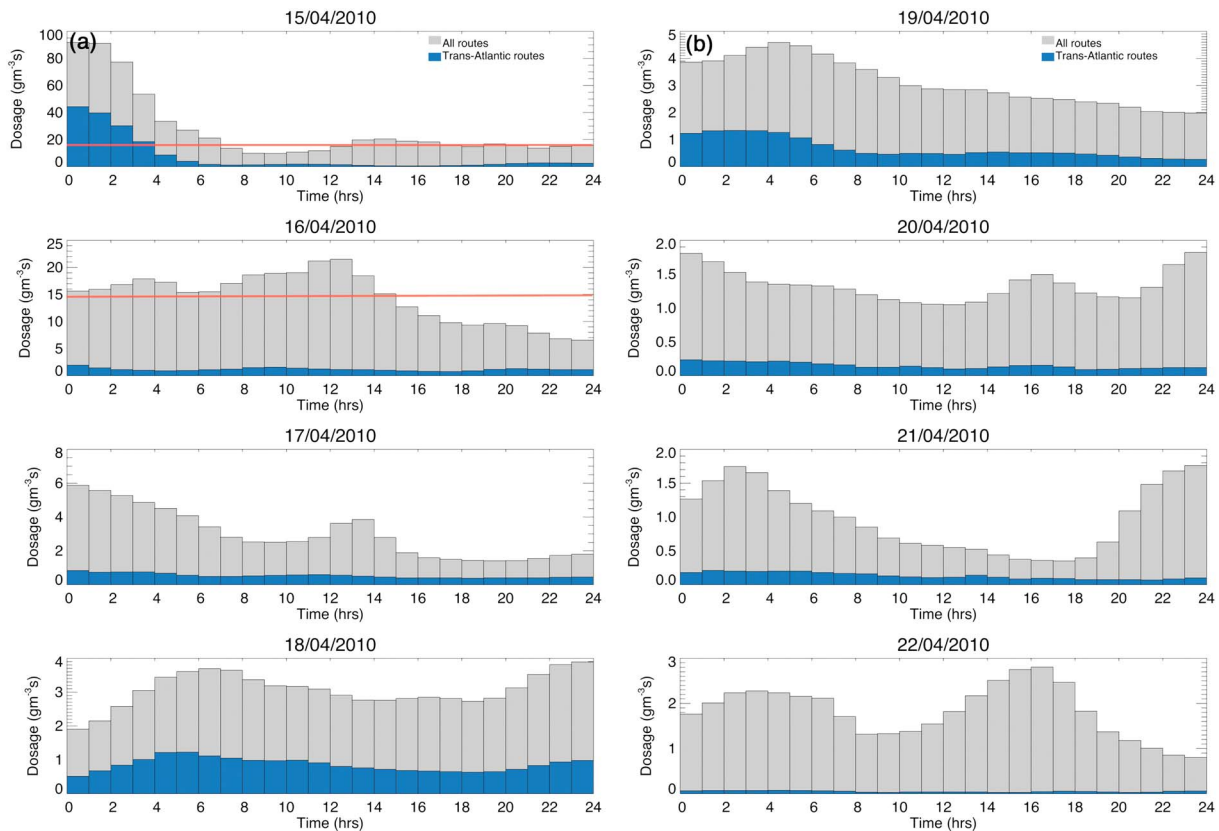
Figure 7. Cumulative dosages for all flight routes and for trans-Atlantic routes by hour and day for (a) 15–18 and (b) 19–22 April. The trans-Atlantic routes are blue. The red lines indicate a dosage of 15 g m^{-3} s.

is more evenly spread throughout the day. In other words, apart from the initial injection of ash into the air routes during the early part of 15 April, it mattered little what time of day an air route was traversed, although there is a falloff during 16–17 April toward the latter part of the day. Notice that the dosages are significantly smaller after 15 April, but aircraft cancelations peaked on 18 April. On 19 April there is a peak between 04:00 and 06:00 UT and a decrease throughout the rest of the day. Although differences in the cumulative amounts are small on 20–22 April there are periods during the day when the hazard is greater or lesser. After 15 April there appears to be no significant difference in the hourly hazard to trans-Atlantic flights. In the third phase of the atmospheric spread of the ash during 5–18 May (see Figure 4) the hourly patterns for both European and trans-Atlantic routes are somewhat different to the earlier phases, principally because the ash moved much further south into the Atlantic, thereby intercepting the North Atlantic Tracks (NATs). From 1 to 4 May mostly European flights are affected, but the ash dosages (and doses, not shown) are low. By 6 May there is a large peak in the dosage in the middle part of the day due to the coincidence of the movement of the ash, by now affecting parts of the UK. On 7 May higher dosages are encountered by trans-Atlantic flights as the ash crossed into the NATs. Between 8 and 11 May the hazard diminished somewhat before another peak on 12 May and a very large peak on 14 May. European flights are mostly affected, but these are dominated by flights across the UK and to and from Iceland with very little hazard evident over continental and eastern Europe. The large peak hazard on 14 May occurs between 04:00 and 10:00 UT, and by rescheduling flights around this time interval the potential risk is reduced by almost a factor of 3. We emphasize here that the actual hazard based on the maximum allowable dosage (or dose) that a commercial jet can safely fly-through is not well known. The latest available information from Rolls-Royce (2016) states "Exposure to a cumulative volcanic ash dose (dosage in our terminology) equivalent to operating for 120 minutes in an actual ash concentration of 2 mg m^{-3} (i.e., 14.4 g m^{-3} s), or lower, should not lead to a significant reduction in engine related flight safety margins if all measures are taken to maximize engine operability margins." This level was not exceeded on any of the flight routes considered in our study.
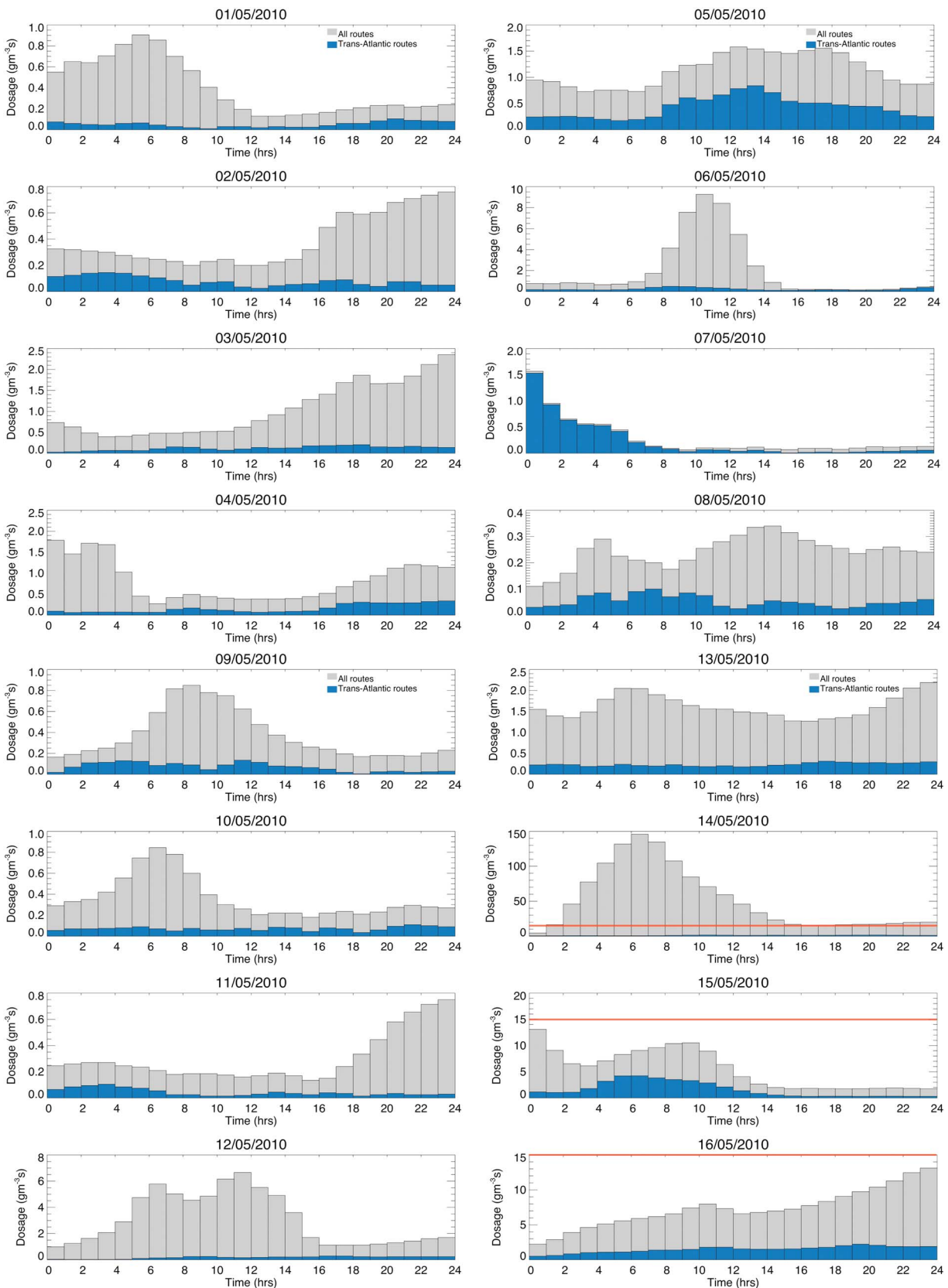
Figure 8. Cumulative dosages for all flight routes and for trans-Atlantic routes by hour and day for 1–16 May. The trans-Atlantic routes are blue. The red lines indicate a dosage of 15 g m^{-3} s.

7. Discussion and Conclusions

About 104,000 flights, with a seat-carrying capacity of ~10 million passengers, were canceled over Europe during the height of the ash crisis in April 2010, and 80% of all flights were canceled on 18 April (Eurocontrol, 2010). Efficient use of models and measurements leads to improved estimates of the aviation hazard posed by dispersing volcanic ash clouds. Here we have used a dispersion model incorporating satellite data via inverse modeling, to provide estimates of doses, dosages, exposures, and dose rates of ash that would have been encountered by commercial aircraft flying from European airports and for some trans-Atlantic destinations during the Eyjafjallajökull ash crisis. The methodology is quite general, and our study could be applied to other eruptions provided a 4-D model/satellite simulation has been made. Such an approach can lead to better contingency planning in the case of future eruptions; for example, flight routes can be adapted to minimize ash dosage while still maintaining necessary airway constraints. Forecast uncertainties, satellite retrieval errors, and the availability of satellite data are limiting factors that must be considered if the methodology is to be used operationally. Forecast errors increase with time, while the density of satellite measurements increases with time and reduces uncertainties in the inversion. These effects have been considered by us (Kristiansen et al., 2012; Seibert et al., 2011) and others (Fu et al., 2017; Wilkins et al., 2016).

The metrics proposed here and the tools used to derive them have certain advantages. They may form a basic set of parameters that can be agreed upon by researchers who determine them, regulators who can use them to help specify safety requirements and airlines who can build them into their safety cases. The tools used to determine the metrics are generic: an atmospheric dispersion model, satellite data, and air route information. Dispersion models are available and used by most Volcanic Ash Advisory Center (VAACs), while satellite data (in near real time) are available at most meteorological centers, which also tend to be the locations of the VAACs. Air route information can be obtained freely, but a better resource is to utilize actual flight plans used by airlines. These data must be obtained through agreement with the airline, but it is in their interest to provide the information. Another advantage of the approach proposed here is that even if the data and forecasts are unavailable during the crisis, a retrospective analysis is valuable. Historical flight data can be used to virtually fly through the model simulation (by now validated and reanalyzed) to provide estimates of exposures, doses, dose rates, and dosages that may have been encountered on routes flown. But the greatest advantage is the use in near real time, where airlines can make rapid assessments based on forecasts and then reroute, cancel, or take other precautions as befits their safety case. The main disadvantages of the approach are that the metrics have not been validated and as yet it is unclear what exposure, dose, dose rate, or dosage is acceptable for safety and economic planning. It may be that a "peak" exposure is a more suitable metric than the current "fixed" concentration levels of 0.2, 2, and 4 mg m^{-3}, or a dose rate not to be exceeded at any time during the flight. Models and observations contain errors, and so the information should be treated like all forecast information as an estimate with uncertainties stated. There is also an issue with timeliness—as an inversion can only be performed when sufficient satellite data are available to perform the inversion. Geostationary infrared satellite data provide the optimal data source because these data are frequent (10–60-min sampling time) and can be used during the day or night. The uncertainties involved in dispersion modeling and ash forecasting have been discussed by Fu et al. (2017), Kristiansen et al. (2012), and Seibert et al. (2011) and others. The metrics and tools should in no way replace current information from VAACs, and other observational information from pilot reports, ground-based, aircraft, and satellite remote sensing. Given that errors are always possible in forecasting dispersion of particulates in the atmosphere and delays in updating information to in-flight aircraft are likely, onboard detection systems still have merit.

For the Eyjafjallajökull ash eruptions during 14 April to 23 May 2010 we found no instances where aircraft traveling along established air routes would have encountered dosages >10 g m^{-3} s, and the majority of dosages encountered were <1 g m^{-3} s. This is mostly due to the fact that the ash clouds were generally lower than the cruise altitudes used by commercial air traffic. Kristiansen et al. (2015) found quite low dosages (~1.2 g m^{-3} s) for an aircraft encounter with an ash cloud from the Kelut eruption, but in this case the ash cloud was very high (>20 km) and it is likely that the aircraft did not penetrate the most concentrated ash clouds. In the case of a larger eruption, sending ash clouds to 30,000 ft or higher, it is very likely that aircraft will be exposed to ash of high concentrations leading to exceedance of dosages of 10 g m^{-3} s. However, for large

Icelandic eruptions that inject ash above 30,000 ft (~9.1 km) the most likely transport direction is zonal and captured within the polar vortex. In terms of the NATs, the worse-case scenario occurs for a high-altitude ash cloud (>9 km) when an upper-level high-pressure ridge forms over the North Atlantic.

References

Dacre, H. F., Grant, A. L., Hogan, R. J., Belcher, S. E., Thomson, D., Devenish, B., et al. (2011). Evaluating the structure and magnitude of the ash plume during the initial phase of the 2010 Eyjafjallajökull eruption using lidar observations and name simulations. *Journal of Geophysical Research*, *116*, D00U03. https://doi.org/10.1029/2011JD015608

Eckhardt, S., Prata, A., Seibert, P., Stebel, K., & Stohl, A. (2008). Estimation of the vertical profile of sulfur dioxide injection into the atmosphere by a volcanic eruption using satellite column measurements and inverse transport modeling. *Atmospheric Chemistry and Physics*, *8*(14), 3881–3897.

Eurocontrol (2010). Ash-cloud of April and May 2010: Impact on air traffic. EUROCONTROL/CND/STATFOR STATFOR/Doc394 (v1.0), 1–45. Retrieved from https://www.eurocontrol.int/sites/default/files/content/documents/official-documents/facts-and-figures/statfor/ash-impact-air-traffic-2010.pdf

Francis, P. N., Cooke, M. C., & Saunders, R. W. (2012). Retrieval of physical properties of volcanic ash using Meteosat: A case study from the 2010 Eyjafjallajökull eruption. *Journal of Geophysical Research*, *117*, D00U09. https://doi.org/10.1029/2011JD016788

Fu, G., Prata, F., Lin, H. X., Heemink, A., Segers, A., & Lu, S. (2017). Data assimilation for volcanic ash plumes using a satellite observational operator: A case study on the 2010 Eyjafjallajökull volcanic eruption. *Atmospheric Chemistry and Physics*, *17*(2), 1187–1205.

Gudmundsson, M. T., Thordarson, T., Höskuldsson, Á., Larsen, G., Björnsson, H., Prata, F. J., et al. (2012). Ash generation and distribution from the April-May 2010 eruption of Eyjafjallajökull, Iceland. *Scientific reports 2*.

Kristiansen, N., Stohl, A., Prata, A., Bukowiecki, N., Dacre, H., Eckhardt, S., et al. (2012). Performance assessment of a volcanic ash transport model mini-ensemble used for inverse modeling of the 2010 Eyjafjallajökull eruption. *Journal of Geophysical Research*, *117*, D00U11. https://doi.org/10.1029/2011JD016844

Kristiansen, N. I., Prata, A., Stohl, A., & Carn, S. A. (2015). Stratospheric volcanic ash emissions from the 13 February 2014 Kelut eruption. *Geophysical Research Letters*, *42*, 588–596. https://doi.org/10.1002/2014GL062307

Millington, S. C., Saunders, R. W., Francis, P. N., & Webster, H. N. (2012). Simulated volcanic ash imagery: A method to compare NAME ash concentration forecasts with SEVIRI imagery for the Eyjafjallajökull eruption in 2010. *Journal of Geophysical Research*, *117*, D00U17. https://doi.org/10.1029/2011JD016770

Naeslund, E., & Thaning, L. (1991). On the settling velocity in a nonstationary atmosphere. *Aerosol Science Technology*, *14*, 247–256.

Pavolonis, M. J. (2010). Advances in extracting cloud composition information from spaceborne infrared radiances — A robust alternative to brightness temperatures. Part I: Theory. *Journal of Applied Meteorology and Climatology*, *49*(9), 1992–2012.

Peterson, R. A., & Dean, K. G. (2008). Forecasting exposure to volcanic ash based on ash dispersion modeling. *Journal of Volcanology and Geothermal Research*, *170*(3), 230–246.

Prata, A., & Grant, I. (2001). Retrieval of microphysical and morphological properties of volcanic ash plumes from satellite data: Application to Mt Ruapehu, New Zealand. *Quarterly Journal of the Royal Meteorological Society*, *127*(576), 2153–2179.

Prata, A., & Prata, A. (2012). Eyjafjallajökull volcanic ash concentrations determined using Spin Enhanced Visible and Infrared Imager measurements. *Journal of Geophysical Research*, *117*, D00U23. https://doi.org/10.1029/2011JD016800

Prata, A., & Rose, W. (2015). Volcanic ash hazards to aviation. Encyclopedia of volcanoes. Chapter 52.

Prata, A. T., Siems, S. T., & Manton, M. J. (2015). Quantification of volcanic cloud top heights and thicknesses using A-train observations for the 2008 Chaitén eruption. *Journal of Geophysical Research: Atmospheres*, *120*, 2928–2950. https://doi.org/10.1002/2014JD022399

Prata, A. T., Young, S. A., Siems, S. T., & Manton, M. J. (2017). Lidar ratios of stratospheric volcanic ash and sulfate aerosols retrieved from CALIOP measurements. *Atmospheric Chemistry and Physics Discussions*, *2017*, 1–28. http://www.atmos-chem-phys-discuss.net/acp-2016-1173/

Rolls-Royce (2016). Volcanic ash limits guidance. WI CR 4 (2-2 (CL) Appendix B3), 1–4. Retrieved from https://www.wmo.int/aemp/sites/default/files/VA_Limits_Guidance_Rolls-Royce.pdf

Seibert, P., Kristiansen, N. I., Richter, A., Eckhardt, S., Prata, A. J., & Stohl, A. (2011). Uncertainties in the inverse modelling of sulphur dioxide eruption profiles. *Geomatics, Natural Hazards and Risk*, *2*(3), 201–216.

Song, W., Lavallée, Y., Hess, K.-U., Kueppers, U., Cimarelli, C., & Dingwell, D. B. (2016). Volcanic ash melting under conditions relevant to ash turbine interactions. *Nature Communications*, *7*, 10795. http://www.nature.com/doifinder/10.1038/ncomms10795

Stohl, A., Prata, A. J., Eckhardt, S., Clarisse, L., Durant, A., Henne, S., et al. (2011). Determination of time- and height-resolved volcanic ash emissions and their use for quantitative ash dispersion modeling: The 2010 Eyjafjallajökull eruption. *Atmospheric Chemistry and Physics*, *11*(9), 4333–4351.

Thomas, H., & Watson, I. (2010). Observations of volcanic emissions from space: Current and future perspectives. *Natural Hazards*, *54*(2), 323–354.

Wilkins, K. L., Watson, I. M., Kristiansen, N. I., Webster, H. N., Thomson, D. J., Dacre, H. F., & Prata, A. J. (2016). Using data insertion with the name model to simulate the 8 May 2010 Eyjafjallajökull volcanic ash cloud. *Journal of Geophysical Research: Atmospheres*, *121*, 306–323. https://doi.org/10.1002/2015JD023895